Ferromagnetic Resonance of Single-Domain Particles*

E. P. VALSTYN,† J. P. HANTON, AND A. H. MORRISH
University of Minnesota, Minneapolis, Minnesota

(Received July 9, 1962)

The ferromagnetic-resonance spectra of powders containing single-domain particles have been studied experimentally and theoretically. The theory is based on the Stoner-Wohlfarth model. The line shapes were calculated with the aid of a high-speed digital computer. Measurements were made on γ-Fe_2O_3 powders, both with and without an applied steady magnetic field. For zero applied steady field, the theoretical line shapes agree well with the experimental ones provided the particle shape distribution, the crystalline anisotropy, and the particle interactions are taken into account. With an applied field, the theoretical curves with only the shape distribution considered do not agree with the theoretical ones. It is found that the anisotropy constant K_1 and the relaxation time τ of γ-Fe_2O_3 are approximately -2.5×10^5 ergs/cm^3 and 2.0×10^{-10} sec, respectively.

INTRODUCTION

AN extensive theoretical and experimental study of ferromagnetic-resonance phenomena in suspensions of single-domain particles, with and without an applied steady magnetic field, has been conducted. The theory is based on the Stoner-Wohlfarth[1] model and takes into account cubic crystalline as well as shape anisotropy; it was assumed that the particles are essentially single crystals of uniaxially symmetrical shape and that the orientation of the particle axis with respect to the crystallographic axes is random. The measurements were made on γ-Fe_2O_3 powders because these can be produced with high purity and different shape distributions. Three powders, which differed from each other by shape distribution and particle size, were investigated. In powder 1, the particle shape was very close to spherical (Fig. 1) and the size ranged from 0.03 to 0.2 μ, the average size being about 0.12 μ. Powders 2 and 3 had acicular particle shapes. Their approximate size and shape distributions had been determined by means of electron photomicrographs previously, in connection with other work.[2] The particle length in these powders ranged from 0.1 to 1.5 μ with a mean between 0.5 and 0.6 μ. In powder 2 the average axial ratio was about 3:1, and in powder 3 it was about 6:1.

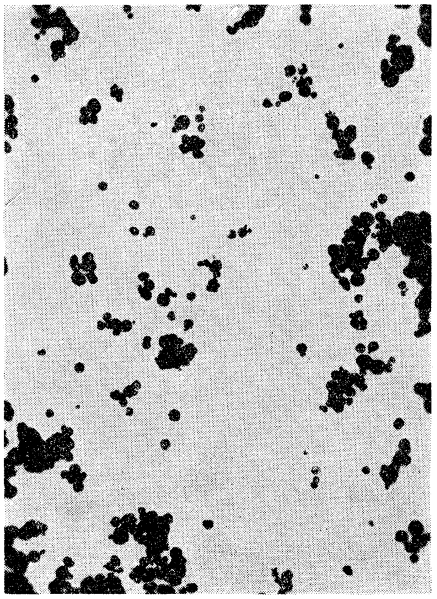

FIG. 1. Electron photomicrograph of powder 1. Magnification 16 150×.

Experiments with acicular single-domain particles which involve irreversible changes of magnetization[3–7] lead to results which disagree strongly with the Stoner-Wohlfarth theory. The hypothesis that these discrepancies are due to incoherent magnetization reversals[8] is supported by the work presented in this paper, where it is shown that ferromagnetic-resonance experiments with single-domain particles, for which nonuniform reversal modes are not likely to be important, yield results which are in reasonably good agreement with the Stoner-Wohlfarth theory even when magnetocrystalline anisotropy and particle interaction are neglected. The agreement is improved by taking into account crystalline anisotropy and particle interaction, the latter by introducing an equivalent change in shape distribution.

From the data, values of the first-order magnetocrystalline anisotropy constant, the relaxation time, and the g factor of γ-ferric oxide are estimated.

THEORY

We first consider an isolated single-domain particle. The problem of ferromagnetic resonance in this par-

* This research was supported by the Air Force Office of Scientific Research of the Office of Aerospace Research, under Contract No. AF 49(638)-803.

† Present address: International Business Machines Corporation, Poughkeepsie, New York.

[1] E. C. Stoner and E. P. Wohlfarth, Phil. Trans. Roy. Soc. (London) **A240**, 599 (1948).

[2] A. H. Morrish and L. A. K. Watt, Phys. Rev. **105**, 1476 (1957).

[3] C. E. Johnson, Jr., and W. F. Brown, Jr., J. Appl. Phys. **29**, 313, 1699 (1958).

[4] A. H. Morrish and S. P. Yu, Phys. Rev. **102**, 670 (1956); A. H. Morrish and L. A. K. Watt, J. Appl. Phys. **29**, 1029 (1958).

[5] C. E. Johnson, Jr., and W. F. Brown, Jr., Suppl. J. Appl. Phys. **30**, 136 (1959).

[6] F. E. Luborsky, Suppl. J. Appl. Phys. **32**, 171 (1961).

[7] W. P. Osmond, Proc. Phys. Soc. (London) **B65**, 121 (1952).

[8] W. F. Brown, Jr., Phys. Rev. **105**, 1479 (1957); E. H. Frei, S. Shtrikman, and D. Treves, *ibid.* **106**, 446 (1957).

ticle is solved in two steps. First, the orientation of the magnetization at static equilibrium is found by minimizing the free energy, F, and then the dynamic part of the problem, the small precessions of the magnetization about its equilibrium orientation, is considered.

If damping is neglected, the equation of motion of the magnetization is

$$d\mathbf{M}/dt=\gamma\mathbf{T}, \tag{1}$$

where $\mathbf{T}$ is the torque acting on the magnetization vector. Let us define a right-handed coordinate system (u,v,r) such that the r direction is in the equilibrium direction of $\mathbf{M}$, which is given by the azimuth ϕ_0 and the polar angle θ_0 (Fig. 2). Let the other two axes be oriented in such a way that $du=-M_s\sin\theta_0 d\phi$ and $dv=M_s d\theta$, M_s being the spontaneous magnetization. Small time-dependent deviations of $\mathbf{M}$ from its equilibrium orientation result in small time-dependent components of $\mathbf{M}$ in the u and v directions, m_u and m_v, corresponding to small angles of deviation ξ and η, respectively, whereas the r component of $\mathbf{M}$ will remain very nearly constant at M_s. We have then the equations of motion:

$$\begin{aligned} M_s\dot{\xi}&=\gamma\partial F/\partial\eta,\\ M_s\dot{\eta}&=-\gamma\partial F/\partial\xi. \end{aligned} \tag{2}$$

Expanding F about the equilibrium position, we have

$$F=F_0+\tfrac{1}{2}(F_{\xi\xi}\xi^2+2F_{\xi\eta}\xi\eta+F_{\eta\eta}\eta^2), \tag{3}$$

where $F_{\xi\xi}$, $F_{\xi\eta}$, and $F_{\eta\eta}$ are the second derivatives at the equilibrium position. Using exponential time dependence for ξ and η, the equations of motion become[9-11]

$$\begin{aligned} j\omega M_s\xi&=\gamma(F_{\xi\eta}\xi+F_{\eta\eta}\eta),\\ -j\omega M_s\eta&=\gamma(F_{\xi\xi}\xi+F_{\xi\eta}\eta). \end{aligned} \tag{4}$$

The set of homogeneous equations (4) has a nontrival solution only when ω is equal to the resonance frequency

$$\begin{aligned} \omega_0&=(\gamma/M_s)(F_{\xi\xi}F_{\eta\eta}-F_{\xi\eta}{}^2)^{1/2}\\ &=(\gamma/M_s\sin\theta_0)(F_{\phi\phi}F_{\theta\theta}-F_{\phi\theta}{}^2)^{1/2}. \end{aligned} \tag{5}$$

Let us now introduce a small alternating field, $\mathbf{h}$, as well as damping. $\mathbf{h}$ exerts a torque $\mathbf{M}\times\mathbf{h}$ on the manetization. Hence, neglecting second-order terms,

$$\begin{aligned} \dot{m}_u&=\gamma(\partial F/\partial\eta)-\gamma M_s h_v-m_u/\tau,\\ \dot{m}_v&=-\gamma(\partial F/\partial\xi)+\gamma M_s h_u-m_v/\tau, \end{aligned} \tag{6}$$

τ being the relaxation time. By using exponential time dependence for $\mathbf{m}$ and $\mathbf{h}$, and on solving for m_u and m_v, we get

$$\begin{aligned} m_u&=\frac{1}{\omega_0{}^2+Z^2}\left[\gamma^2F_{\theta\theta}h_u+\left(\frac{\gamma^2F_{\phi\theta}}{\sin\theta_0}-\gamma M_sZ\right)h_v\right],\\ m_v&=\frac{1}{\omega_0{}^2+Z^2}\left[\left(\frac{\gamma^2F_{\phi\theta}}{\sin\theta_0}+\gamma M_sZ\right)h_u+\frac{\gamma^2F_{\phi\phi}}{\sin^2\theta_0}h_v\right], \end{aligned} \tag{7}$$

[9] J. Smit and H. G. Beljers, Philips Research Repts. **10**, 113 (1955).
[10] H. Suhl, Phys. Rev. **97**, 553 (1955).
[11] H. Zeiger (unpublished).

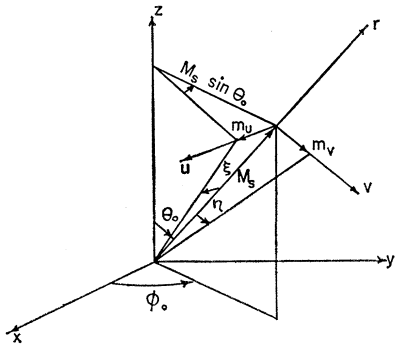

FIG. 2. Small deviations of $\mathbf{M}$ from its equilibrium orientation, (ϕ_0,θ_0).

where $Z=\tau^{-1}+j\omega$. The extrinsic susceptibility tensor, which relates $\mathbf{m}$ to the external high-frequency field, $\mathbf{h}$, is defined by $\mathbf{m}=\chi\cdot\mathbf{h}$. Hence,

$$\chi=\begin{bmatrix}\chi_{uu} & \chi_{uv} & 0\\ \chi_{vu} & \chi_{vv} & 0\\ 0 & 0 & 0\end{bmatrix},$$

$$\chi_{uu}=\frac{\gamma^2F_{\theta\theta}}{\omega_0{}^2+Z^2},\quad \chi_{uv}=\frac{1}{\omega_0{}^2+Z^2}\left(\frac{\gamma^2F_{\phi\theta}}{\sin\theta_0}-\gamma M_sZ\right), \tag{8}$$

$$\chi_{vu}=\frac{1}{\omega_0{}^2+Z^2}\left(\frac{\gamma^2F_{\phi\theta}}{\sin\theta_0}+\gamma M_sZ\right),\quad \chi_{vv}=\frac{\gamma^2F_{\phi\phi}}{(\omega_0{}^2+Z^2)\sin^2\theta_0}.$$

The "scalar" susceptibility, χ, is defined by $m_h=\chi h$, where m_h is the component of $\mathbf{m}$ in the direction of $\mathbf{h}$, i.e.,

$$\chi=(1/h^2)(\mathbf{h}^*\cdot\mathbf{m})=(1/h^2)(\mathbf{h}^*\cdot\chi\cdot\mathbf{h}). \tag{9}$$

We find then

$$\chi=\frac{\gamma^2}{\omega_0{}^2+Z^2}\left(F_{\theta\theta}l^2+\frac{F_{\phi\phi}m^2}{\sin^2\theta_0}+\frac{2F_{\phi\theta}lm}{\sin\theta_0}\right), \tag{10}$$
$$l=h_u/h,\quad m=h_v/h.$$

Suppose now that the x, y, and z axes in Fig. 2 are the principal cubic axes and let us define directions with respect to this coordinate system by azimuths and polar angles as shown in Fig. 3. We find then

$$\begin{aligned} l&=\sin\rho\sin(\phi_0-\lambda),\\ m&=\sin\rho\cos\theta_0\cos(\phi_0-\lambda)-\cos\rho\sin\theta_0. \end{aligned} \tag{11}$$

When discussing ferromagnetic resonance in a single-domain particle and neglecting strains, three contributions to the free energy must, in general, be considered[12]: the contribution due to a steady field acting on the particle,

$$\begin{aligned} F_H&=-\mathbf{H}\cdot\mathbf{M}\\ &=-HM_s[\sin\sigma\sin\theta\cos(\psi-\phi)+\cos\sigma\cos\theta]; \end{aligned} \tag{12}$$

[12] N. Bloembergen, Proc. Inst. Radio Engrs. **44**, 1259 (1956).

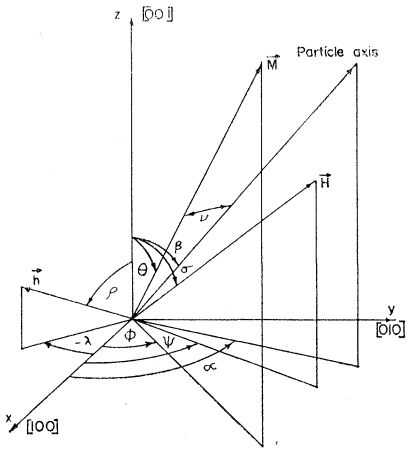

FIG. 3. Azimuths and polar angles defining the orientations of **H**, **h**, **M**, and the particle axis.

the demagnetizing energy,

$$F_N=\tfrac{1}{2}\mathbf{M}\cdot\mathbf{N}\cdot\mathbf{M}=\tfrac{1}{2}M_s^2N_b$$
$$-\tfrac{1}{2}M_s^2\eta[\sin^2\beta\sin^2\theta\cos^2(\alpha-\phi)+\cos^2\beta\cos^2\theta$$
$$+\tfrac{1}{2}\sin 2\beta\sin 2\theta\cos(\alpha-\phi)], \quad (13)$$

where **N** is the demagnetizing tensor, N_a the axial, and N_b the transverse demagnetizing factor of a spheroid, and where we have defined the shape factor $\eta=N_b-N_a$; finally, the magnetocrystalline anisotropy energy,

$$F_K=K_1(\alpha_1^2\alpha_2^2+\alpha_2^2\alpha_3^2+\alpha_3^2\alpha_1^2)$$
$$=\tfrac{1}{4}K_1(\sin^2 2\phi\sin^4\theta+\sin^2 2\theta), \quad (14)$$

where higher-order terms are neglected and where α_1, α_2, and α_3 are the direction cosines of **M** with respect to the principal cubic axes.

To find the susceptibility of a powder consisting of single-domain particles, one must make some assumptions concerning the orientation of the particle axes and the crystallographic axes in space. Suppose a suspension of the powder has been prepared in such a way that one can assume random orientation of the particle axes in space. For powder 1, it is reasonable to assume that the particles are single crystals. However, electron diffraction experiments with acicular γ-Fe_2O_3 particles carried out by Campbell[13] seem to indicate that the particles are polycrystalline, although there is no conclusive proof. On the other hand, acicular particles were considered as single crystals by Wohlfarth and Tonge.[14] Campbell[13] found that most of the particles have a definite crystallographic direction along the particle axis, but that there may be random orientation about the particle axis. The crystallographic direction along the particle axis was usually of low order, e.g., [111], [211], [221], [331], etc., but there was no indication that any one direction predominates. Hence, when the bulk properties of the powder are considered, random orientation of the particle axes with respect to the principal cubic axes is a reasonable assumption. Furthermore, we consider the particles to be essentially single crystals.

With random particle orientation, the individual particle can be regarded as being located at the center of a spherical cavity in a homogeneous, isotropic medium with intrinsic susceptibility χ_p. Some of the particles of the powder will be so close to the one under consideration that they must be considered as lying inside the spherical cavity. If the shape of the powder sample is ellipsoidal, the time-varying field and magnetization outside the cavity, $\mathbf{h}_p$ and $\mathbf{m}_p$, are homogeneous. The time-dependent field acting on the particle is then

$$\mathbf{h}=\mathbf{h}_p+N_s\mathbf{m}_p+\mathbf{h}_i,$$

where N_s is the demagnetizing factor of a sphere and $\mathbf{h}_i$ is the field due to the particles inside the spherical cavity. $\mathbf{h}_i$ changes in magnitude and direction from one particle to the other, the direction being random. If the powder sample is spherical and a homogeneous time-dependent field $\mathbf{h}_e$ is applied to it, $\mathbf{m}=\boldsymbol{\chi}\cdot\mathbf{h}_e+\boldsymbol{\chi}\cdot\mathbf{h}_i$. Now consider all particles with the same $\boldsymbol{\chi}$, which is independent of **h**. Their average magnetization is $\boldsymbol{\chi}\cdot\mathbf{h}_e$, since the direction of $\mathbf{h}_i$ is random; and so the "scalar" susceptibility relating their average magnetization to $\mathbf{h}_e$ is, by (9),

$$\chi=(1/h_e^2)\mathbf{h}_e^*\cdot\boldsymbol{\chi}\cdot\mathbf{h}_e.$$

This leads to (10), where now l and m are the direction cosines of $\mathbf{h}_e$. When χ is averaged over all particles in the powder, and multiplied by the volume concentration, p, one obtains the extrinsic susceptibility of a spherical powder sample, χ_e. In this, one is faced with the difficulty that **H**, the steady field to which the particle is subjected, varies in direction and magnitude from one particle to the other and that the effect of this variation does not average out, as is the case with the alternating field. If $\mathbf{H}_e$ is the steady field applied externally to the spherical powder sample,

$$\mathbf{H}=\mathbf{H}_e+\mathbf{H}_i, \quad (15)$$

where $\mathbf{H}_i$ is the steady field due to the presence of particles inside the spherical cavity surrounding the particle considered. As far as the powder as a whole is concerned, the direction of $\mathbf{H}_i$ can be assumed to be random, but the magnitude follows a distribution function, $G(H_i)$, which must be calculated or assumed if it is desired to take account of particle interaction.

Let us neglect particle interaction for the time being, i.e., let us set $\mathbf{H}=\mathbf{H}_e$; then

$$\chi_e=\frac{p}{64\pi^3}\int_0^{2\pi}d\alpha\int_0^{\pi}\sin\beta d\beta\int_0^{2\pi}d\psi\int_0^{\pi}\sin\sigma d\sigma$$
$$\times\int_0^{2\pi}d\lambda\int_0^{\pi}\sin\rho d\rho\int_0^{2\pi}\chi\Phi(\eta)d\eta, \quad (16)$$

[13] R. B. Campbell, "Report of A.I.E.E. Conference on Magnetism and Magnetic Materials," Boston, Mass., October, 1956 [A.I.E.E. Publication T-91 (unpublished)]; p. 128.
[14] E. P. Wohlfarth and D. G. Tonge, Phil. Mag. **3**, 536 (1958).

where $\Phi(\eta)$ is the shape distribution of the particles in the powder. Whether this is the susceptibility measured in a particular experiment depends on the nature of the experiment. The cavity method measures the extrinsic susceptibility of the sample.[15] However, any method which employs toroidal or ring-shaped samples[16] determines the intrinsic susceptibility of the powder, χ_p, since demagnetizing fields are absent with such an experimental arrangement.[17] For a spherical powder sample, $m_p=\chi_p h_p=\chi_e h_e$. Hence,

$$\chi_e=\chi_p/(1+N_s\chi_p),$$

or

$$\mu_e'-1=\frac{\mu_p'-1+\frac{1}{3}|\mu_p-1|^2}{1+\frac{2}{3}(\mu_p'-1)+\frac{1}{9}|\mu_p-1|^2},$$
$$\mu_e''=\mu_p''/[1+\tfrac{2}{3}(\mu_p'-1)+\tfrac{1}{9}|\mu_p-1|^2] \quad (17)$$

for all systems of units.

Zero Applied Steady Field ($\mathbf{H}_e=0$)

In this case, since particle interaction is neglected, $F_H=0$. If the powder is in the demagnetized state, Eq. (16) becomes[18]

$$\chi_e=\frac{p\gamma^2}{12\pi}\int_0^{2\pi}\Phi(\eta)d\eta\int_0^{2\pi}d\alpha\int_0^{\pi}\left[\frac{F_{\theta\theta}+F_{\phi\phi}/\sin^2\theta_0}{\omega_0^2+Z^2}\right]\times\sin\beta d\beta. \quad (18)$$

If, in addition, the particle shape is spherical (powder 1), F_N is independent of θ and ϕ and

$$\chi_e=[p\gamma^2/3(\omega_0^2+Z^2)][F_{K\theta\theta}+F_{K\phi\phi}/\sin^2\theta_0]. \quad (19)$$

Let us assume that $K_1<0$, as is the case in γ-Fe_2O_3; then, in the absence of shape anisotropy, the minima of the energy surface are in the [111] directions, all corresponding to the same resonance frequency, $\omega_0=(4\gamma/3)\times(|K_1|/M_s)$, and (19) becomes

$$\chi_e=(8/9)[p\gamma^2|K_1|/(\omega_0^2+Z^2)]. \quad (19a)$$

When the particles of a single-domain powder are highly acicular and the crystalline anisotropy is low, one can, in the first approximation, set $F_K=0$, so that $F=F_N$. Then

$$\chi_e=\tfrac{2}{3}p\gamma^2M_s^2\int_0^{2\pi}\frac{\Phi(\eta)d\eta}{\gamma^2M_s^2\eta^2+Z^2}. \quad (20)$$

Steady Field Applied ($\mathbf{H}_e\neq0$)

In the presence of a steady field as well as shape and crystalline anisotropy, Eq. (16) cannot be brought into any form that would facilitate discussion or numerical analysis. If crystalline anisotropy can be neglected, i.e., $F=F_H+F_N$, a not too unwieldy expression for χ_e can be derived.[18] The conditions for stable equilibrium are then[1]

$$\phi_0=\alpha=\psi,$$
$$M_s\eta\sin2(\beta-\theta_0)=2H_e\sin\theta_0, \quad (21)$$
$$M_s^2\eta\cos2(\beta-\theta_0)+H_eM_s\cos\theta_0>0,$$

and

$$\chi_e''=\frac{pD}{4}\int_0^{2\pi}\Phi(\eta)d\eta\times\int_0^{\pi}\frac{[R(1+\cos^2\theta_0)+\eta(\cos2\delta+\cos^2\delta\cos^2\theta_0)]\sin\beta d\beta}{[R^2+R\eta(3\cos^2\delta-1)+\eta^2\cos^2\delta\cos2\delta+B]^2+D^2}, \quad (22)$$

where $\delta=\beta-\theta_0$, $R=(H_e/M_s)\cos\theta_0$, $B=(1-\omega^2\tau^2)/\tau^2\gamma^2M_s^2$, and $D=2\omega/\tau\gamma^2M_s^2$.

NUMERICAL ANALYSIS

The Control Data Corporation 1604 high-speed digital computer was used to obtain the theoretical results. Three programs were prepared. Program 1 evaluates χ_e' and χ_e'' for $H_e=0$ and $K_1=0$, i.e., it is based on Eq. (20). Program 2 computes χ_e' and χ_e'' from Eq. (18), i.e., $H_e=0$ but crystalline as well as shape anisotropy are taken into account. Program 3 evaluates χ_e'' in Eq. (22); here, a steady field is applied and crystalline anisotropy is neglected.

The particles in powders 2 and 3 were considered to have the shape of right cylinders. Brown and Morrish[19] have shown that, as far as behavior of the magnetization is concerned, an arbitrarily shaped single-domain particle is equivalent to one with the shape of a suitably chosen ellipsoid; hence, the shape factor, $\eta=N_b-N_a$, can be calculated for any single-domain particle of uniaxially symmetrical shape. The shape factors of right cylinders with different axial ratios were obtained from tables computed by Brown.[20]

Our computed results are strongly affected by the value used for M_s, the spontaneous magnetization of γ-Fe_2O_3 at room temperature, since F_N is proportional to M_s^2. Birks[21] used 350 emu/cm³ for M_s, whereas Brown, Hanton, and Morrish[22] employed 390 emu/cm³. In our first computations, M_s was made equal to 390 emu/cm³. Later, our attention was called to what was at that time an unpublished paper[23] according to which 370 emu/cm³ is a better value, and this was then used in the remaining work.

---

[15] R. F. Soohoo, *Theory and Application of Ferrites* (Prentice Hall, Inc., Englewood Cliffs, New Jersey, 1960), pp. 92 and 262.
[16] J. Smit and H. P. J. Wijn, *Ferrites* (John Wiley & Sons, Inc., New York, 1959), pp. 100–103.
[17] J. Smit and H. P. J. Wijn, reference 16, pp. 4 and 121.
[18] E. P. Valstyn, Ph.D. thesis, University of Minnesota, 1962 (unpublished).
[19] W. F. Brown, Jr., and A. H. Morrish, Phys. Rev. **105**, 1198 (1957).
[20] W. F. Brown, Jr. (private communication).
[21] J. B. Birks, Proc. Phys. Soc. (London) **B63**, 65 (1950).
[22] W. F. Brown, Jr., J. P. Hanton and A. H. Morrish, Suppl. J. Appl. Phys. **31**, 214 (1960).
[23] W. F. Brown, Jr., and C. E. Johnson, Jr., J. Appl. Phys. **33**, 2752 (1962). Also see W. E. Henry and M. J. Boehm, Phys. Rev. **101**, 1253 (1956).

In all computations, the g factor was made equal to 2. This is a reasonable assumption, since in γ-Fe_2O_3 the magnetic moments are those of the Fe^{3+} ions, which have a ^6S ground state. It is also supported by the experimental results with an applied steady field (see below).

EXPERIMENTS

All measurements were carried out at room temperature. For zero applied steady field, the real and imaginary parts, μ_p' and μ_p'', of the intrinsic permeability of powders 1, 2, and 3 were determined as a function of frequency between zero and 12 kMc/sec (Fig. 4). The powders were suspended in paraffin wax, their volume concentration being 0.15. Below 25 Mc/sec, a toroidal coil wound on a toroidal sample of the suspension was connected in a bridge circuit.[24,25] Above 200 Mc/sec, the "thin sample" method[26,27] was used, in which a thin, ring-shaped sample is placed on the shorting plunger of a coaxial line. No measurements were made in the range between 25 and 200 Mc/sec. For the purpose of comparison with our theoretical results, μ_e' and μ_e'' were computed from the experimentally determined values of μ_p' and μ_p'', using Eq. (17) and the resulting curves are shown in Fig. 5.

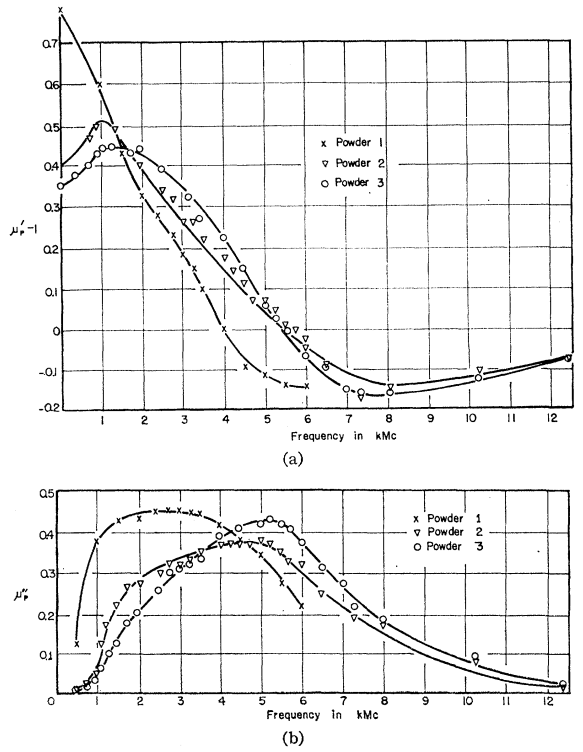

FIG. 4. (a) $\mu_p'-1$ and (b) μ_p'' for powders 1, 2, and 3 at room temperature and zero applied steady field.

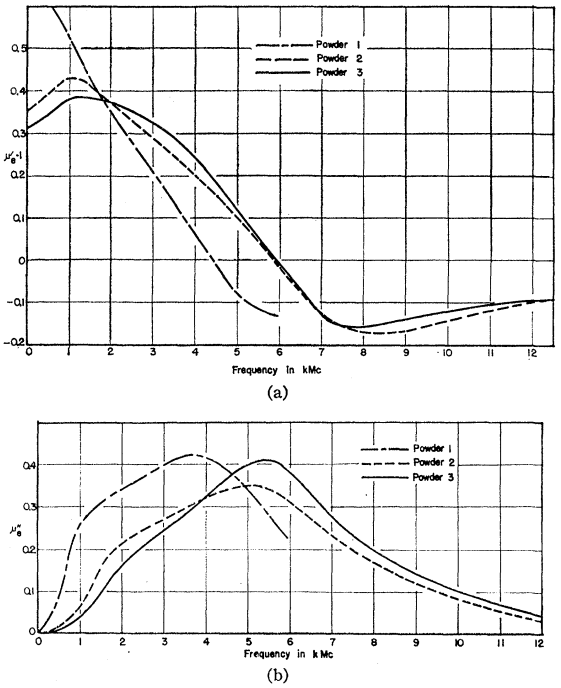

FIG. 5. (a) $\mu_e'-1$ and (b) μ_e'' for powders 1, 2, and 3 at room temperature and zero applied steady field.

The cavity method[15] was used to determine the shape of $\chi_e''(H_e)$ at two frequencies: 9480 Mc/sec and 24 116 Mc/sec. Rectangular transmission and reflection cavities were employed.[18] The preparation of the spherical powder samples has been described elsewhere.[28]

DISCUSSION OF RESULTS

Zero Applied Steady Field ($\mathbf{H}_e=0$)

The most striking feature of the μ_e'' curves are the humps on the low-frequency side, which are more prominent the less acicular the particles of the powder are. These humps can only occur when the effect of the crystalline anisotropy is comparable to that of the shape anisotropy. When the crystalline anisotropy is negligible, the resonance frequency, ω_0, is directly proportional to η ($\omega_0=\gamma M_s\eta$) and, hence, for shape distributions like those of powders 2 and 3, the low-frequency humps cannot occur. On the other hand, when crystalline anisotropy alone is present, there is only one resonance frequency, $\omega_0=(4\gamma/3)(|K_1|/M_s)$. However, when both crystalline and shape anisotropy must be considered, the resonance frequency depends not only on K_1 and η, but also on the orientation of the particle axis with respect to the crystallographic axes. For an arbitrary particle orientation (see Appendix, Table III), a particle with sufficiently low shape factor has four different resonance frequencies[29]; there are eight

[24] R. F. Soohoo, reference 15, p. 101.
[25] J. P. Hanton, M.S. thesis, University of Minnesota, 1959 (unpublished).
[26] W. E. Swanson, M.S. thesis, University of Minnesota, 1957 (unpublished).
[27] G. T. Rado, V. J. Folen, and W. H. Emerson, Proc. Inst. Elec. Engrs. **104B**, Suppl. 5, 198 (1957).
[28] E. P. Valstyn, A. H. Morrish, and C. W. Searle, Rev. Sci. Instr. **33**, 377 (1962).
[29] Of course, the indidivual particle can resonate at only one of these frequencies, since the magnetization can assume only one

energy minima, which change their positions within their octants as the shape factor is increased from zero; they disappear in pairs, each pair corresponding to one value of ω_0, as η is increased, until finally only two minima and, hence, only one resonance frequency remains. Figure 6 shows the minima of $F=F_N+F_K$ for $\alpha=0°$, $\beta=30°$, and particles of different acicularity, as well as the corresponding resonance frequencies (also see Appendix, Table II). In this case, the minima in octants 1 and 4 merge and then move together towards the particle axis. From all these results it can be seen that for $K_1=-3.0\times10^5$ ergs/cm^3, i.e., for a comparatively strong crystalline anisotropy, a relatively large number of particles with medium acicularity have rather low resonance frequencies. This is a qualitative explanation of the experimental results for powders 2 and 3, but not for those of powder 1. For, if the crystalline anisotropy is so large that it strongly affects the behavior of even the most acicular powder, it certainly must completely dominate the small shape anisotropy of powder 1. Hence, each particle in powder 1 should have the same value of ω_0 and there should be no low-frequency hump. In fact, the line shape should be rather narrow (see curve S in Fig. 8). But, this is true only when particle interaction is negligible.

By neglecting interaction between particles, we have set $\mathbf{H}_i$ in Eq. (15) equal to zero. This will probably not unduly influence the theoretical results when an applied steady field, $\mathbf{H}_e$, of several thousand oersteds is present. However, when $\mathbf{H}_e=0$, the effect of particle interaction will be noticeable. This point was investigated experimentally. A sample was prepared by intimately mixing nonmagnetic acicular particles of $FeO\cdot OH$ with Al_2O_3, and then by reducing the particles to γ-Fe_2O_3. Such a technique removes or reduces the clumping of the magnetic particles, and hence decreases the interaction effects. The maximum of the initial permeability of this sample occurred at a slightly higher frequency than that of a normal sample (γ-Fe_2O_3 powder suspended in paraffin). As will be seen from the following discussion, this is the result expected.

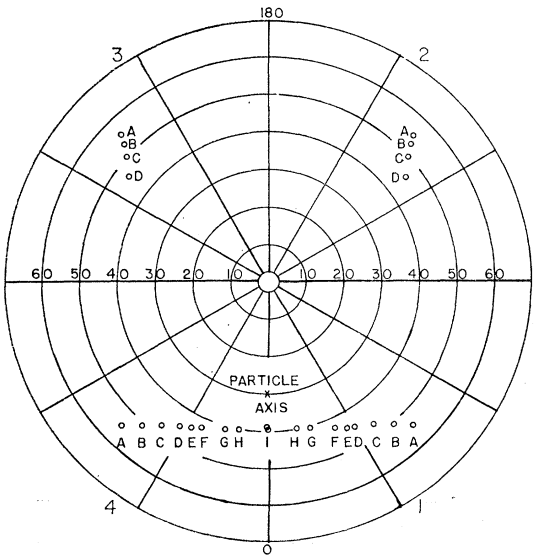

FIG. 6. Minima of $F=F_N+F_K$ on the unit sphere for $\alpha=0°$, $\beta=30°$, $M_s=390$ emu/cm^3, $K_1=-3.0\times10^5$ ergs/cm^3, and $g=2.00$. The axial ratio (spheroid) and resonance frequency for each minimum shown is indicated by the corresponding letter in Table II in the Appendix.

equilibrium position. It is reasonable to assume, however, that in a powder all resonance frequencies will occur and that none of them will be preferred.

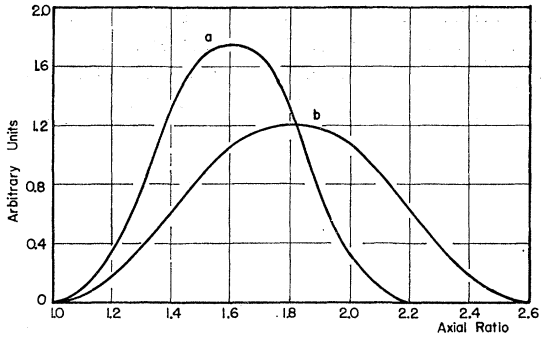

FIG. 7. Effective shape distributions for powder 1. The axial ratios are those of spheroids.

A field, such as $\mathbf{H}_i$, acting on a spherical particle has an effect on the free energy very similar to that of a uniaxial shape anisotropy with $\eta>0$, which tends to pull the magnetization vector away from the [111] directions and closer to the particle axis. An increase in η corresponds to an increase in H_i. In order to make use of program 2, one can, therefore, assume that the randomly oriented field $\mathbf{H}_i$ with a magnitude distribution $G(H_i)$ is equivalent to an effective shape distribution $\Phi(\eta_e)$ of randomly oriented particles. In this way, the low-frequency hump in the μ_e'' curve of powder 1 can be explained. To show this quantitatively, several effective shape distributions were assumed and program 2 was used to compute μ_e' and μ_e'' as a function of frequency, trying different values for K_1 and τ. The best results were obtained with the two effective shape distributions shown in Fig. 7 and by setting $K_1=-2.5\times10^5$ ergs/cm^3 and $\tau=1.9\times10^{-10}$ sec. In Fig. 8, these results, as well as some other computed curves, can be compared with the experimental data. It will be noticed that the theoretical curves for $\mu_e'-1$ have a rather prominent knee and that a similar, but less noticeable knee is present in the experimental curves.

Figures 9 and 10 show the theoretical results obtained for the acicular powders. The curves designated with X were obtained by using program 1 and, hence, Eq. (20), i.e., neglecting crystalline anisotropy. As could be expected, the agreement with experiment is only very rough, especially as far as the $\mu_e'-1$ curves are concerned.

A rather strong crystalline anisotropy had to be assumed to make the line shape change appreciably; setting $K_1=-0.5\times10^5$ ergs/cm^3, for instance,[21] had almost no effect on the shape of the curves. The com-

puted results for $K_1=-2.5\times10^5$ ergs/cm³, $M_s=390$ emu/cm³, and $\tau=1.5\times10^{-10}$ sec are shown in Figs. 9 and 10 (curves designated with Y). For powder 2, the agreement with experiment has been somewhat improved, but this is not true for powder 3. Higher anisotropy constants were tried, but made matters worse; in particular, the peaks of the μ_e'' curves moved to higher frequencies as $|K_1|$ was increased. Even when 370 emu/cm³ was finally used for the spontaneous magnetization, the low-frequency humps in the μ_e'' curves did not appear.

It seems that a better agreement with experiment can only be achieved if particle interaction is taken into account. Again, to make use of program 2, one can assume that the effect of the interaction field, $\mathbf{H}_i$, on the energy surface of a particle is equivalent to a change in the shape factor, η. This, of course, can only be a rough approximation of the physical situation; for in order to stimulate with some accuracy the effects of both the actual (uniaxial) particle shape and the field $\mathbf{H}_i$, the effective particle shape could, in general, not have uniaxial symmetry and, hence, an effective shape factor, η_e, would have no clearly defined meaning, since there are now three different demagnetizing factors.

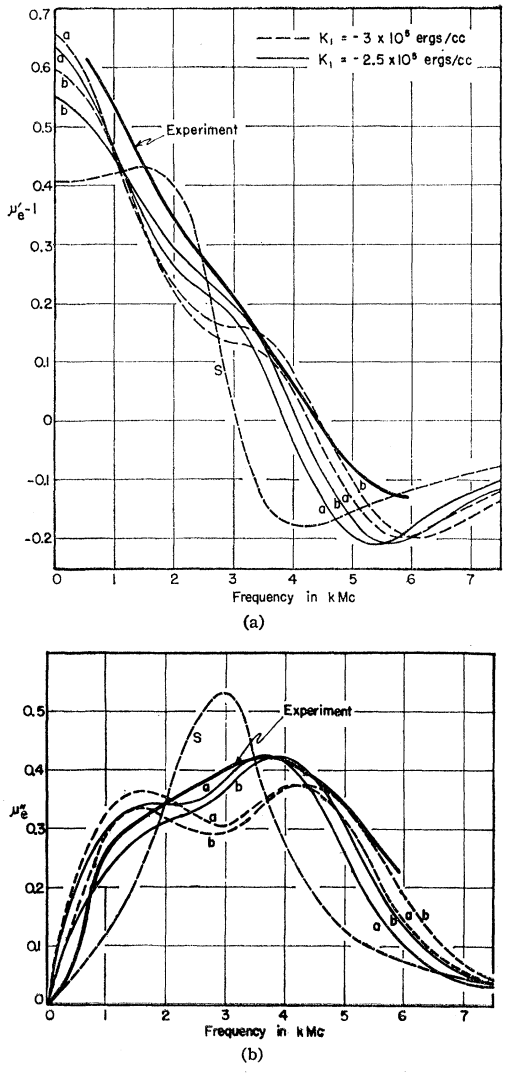

FIG. 8. (a) $\mu_e'-1$ and (b) μ_e'' for powder 1. The letters a and b refer to the effective shape distributions in Fig. 4. Curve S is for $\eta=0$, $K_1=-3.0\times10^5$ ergs/cm³, and $\tau=1.3\times10^{-10}$ sec and has been computed from Eq. (19a).

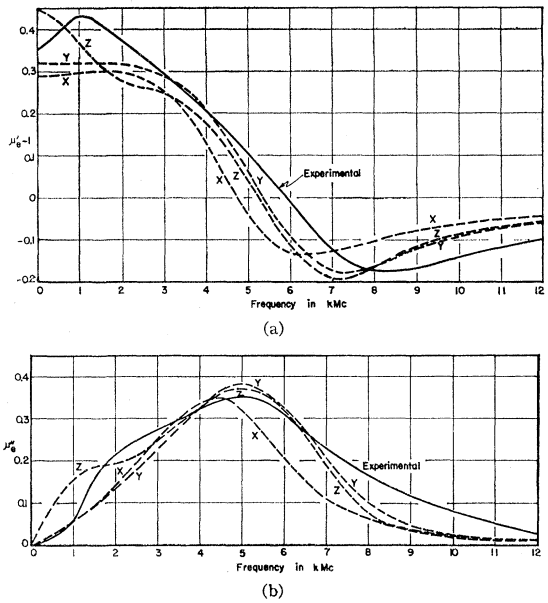

FIG. 9. (a) $\mu_e'-1$ and (b) μ_e'' curves for powder 2. X: $M_s=390$ emu/cm³, $\tau=1.0\times10^{-10}$ sec, $K_1=0$. Y: $M_s=390$ emu/cm³, $\tau=1.5\times10^{-10}$ sec, $K_1=-2.5\times10^5$ ergs/cm³. Z: $M_s=370$ emu/cm³, $\tau=1.9\times10^{-10}$ sec, $K_1=-3.0\times10^5$ ergs/cm³, $k_r=0.9$.

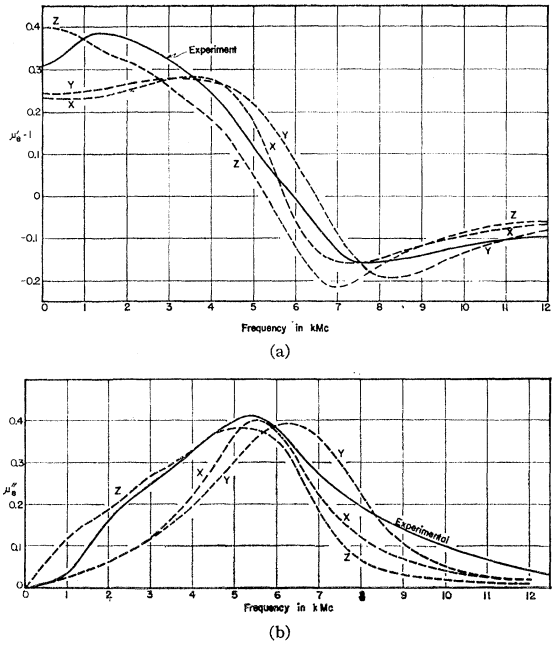

FIG. 10. (a) $\mu_e'-1$ and (b) μ_e'' curves for powder 3. X: $M_s=390$ emu/cm³, $\tau=1.0\times10^{-10}$ sec, $K_1=0$. Y: $M_s=390$ emu/cm³, $\tau=1.5\times10^{-10}$ sec, $K_1=-2.5\times10^5$ ergs/cm³. Z: $M_s=370$ emu/cm³, $\tau=1.9\times10^{-10}$ sec, $K_1=-3.0\times10^5$ ergs/cm³, $k_r=0.7$.

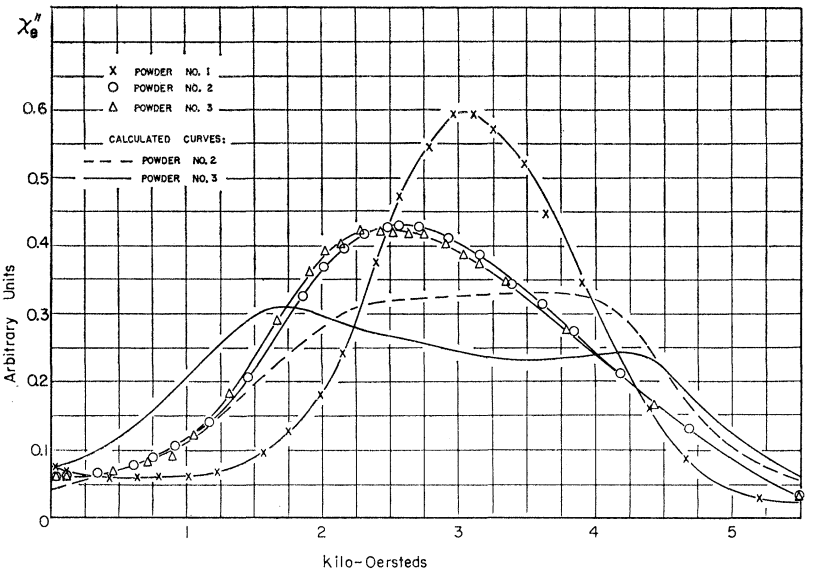

FIG. 11. Theoretical and experimental results for 9480 Mc/sec.

Let us, however, assume that there is an effective shape factor for each particle. When $\mathbf{H}_i$ lies along the particle axis, or when the angle between $\mathbf{H}_i$ and the particle axis is small, then $\eta_e > \eta$; otherwise $\eta_e < \eta$. Hence, if one assumes random orientation of $\mathbf{H}_i$ with respect to the particle axis, the great majority of the particles in an acicular powder can be considered to have an effective shape factor which is smaller than the actual one. One would expect this effective reduction of the shape factor to be the greater the more acicular the particles are.

Again taking an oversimplified approach to a complex problem, a reduction coefficient, k_r, was introduced, by which the shape factors of all the particles in a certain powder were multiplied. The best results were achieved by choosing $k_r = 0.9$ for powder 2 and $k_r = 0.7$ for powder 3. As was the case for powder 1, $|K_1|$ had to be made very large in order to obtain any low-frequency humps in the μ_e'' curves. The curves marked with Z in Figs. 9 and 10 were obtained with $K_1 = -3.0\times10^5$ ergs/cm^3, $M_s = 370$ emu/cm^3, and $\tau = 1.9\times10^{-10}$ sec. As was to be expected after all the assumptions and simplifications made, agreement with experiment is not really good. In the μ_e'' curves the low-frequency humps are not where they should be and the high-frequency branches fall off too abruptly. The latter feature is due to the fact that we have reduced the shape factor of all the particles in a powder by the same factor, k_r. This is a very crude simplification, since for some particles, namely, for those in which the angle between $\mathbf{H}_i$ and the particle axis is small, the effective shape factor will even be greater than the actual one. It will be noticed the $\mu_e' - 1$ curves designated with Z would be very close to each other if they appeared on the same drawing, and this agrees well with experiment.

Steady Field Applied ($\mathbf{H}_e \neq 0$)

The results obtained with the cavity method and in the presence of an applied steady field for spherical samples of randomized powders, with a volume concentration of 0.15, are shown in Figs. 11 and 12. The ine shape of powder 1 is almost symmetrical; however, there is a slight asymmetry, the low-field branch of the curve being steeper than the high-field branch, which indicates a negative first-order cubic anisotropy constant.[30]

The theoretical curves in Figs. 11 and 12 were computed with the aid of program 3, using $M_s = 390$ emu/cm^3 and $\tau = 1.0\times10^{-10}$ sec. Program 3 is based on Eq. (22), in which crystalline anisotropy is neglected, and this is probably the cause of the disagreement between the experimental data and the computed curves. All the results for $\mathbf{H}_e = 0$ indicate that, in powders 2 and 3, the effect of crystalline anisotropy is comparable to that of shape anisotropy and, hence, one would expect poor agreement with experiment when crystalline anisotropy is neglected. However, a computer program taking into account both crystalline and shape anisotropy as well as the applied steady field would be rather complex and was not attempted.

For a system of randomly oriented, noninteracting spherical crystallites with cubic anisotropy, a first-order approximation gives a resonance field[30–32]

$$H_r = (\omega/\gamma) + K_1/2M_s, \tag{23}$$

and a line width increase of $|K_1/M_s|$. Hence, since the particle shape of powder 1 was very close to spherical and measurements were made at two widely separated frequencies, it was possible to estimate the g factor, K_1, and the relaxation time, τ, of γ-Fe_2O_3. The value of τ arrived at in this way must be considered a lower limit, since particle interaction and slight deviations from spherical particle shape also contribute to the

[30] E. Schlömann, "Report of the A.I.E.E. Conference on Magnetism and Magnetic Materials," Boston, Mass., October, 1956 [A.I.E.E. Publication T-91 (unpublished)]; p. 600.
[31] J. H. van Vleck, Phys. Rev. **78**, 266 (1950).
[32] D. M. S. Bagguley, Proc. Phys. Soc. (London) **A66**, 765 (1953); Proc. Roy. Soc. (London) **A228**, 549 (1955).

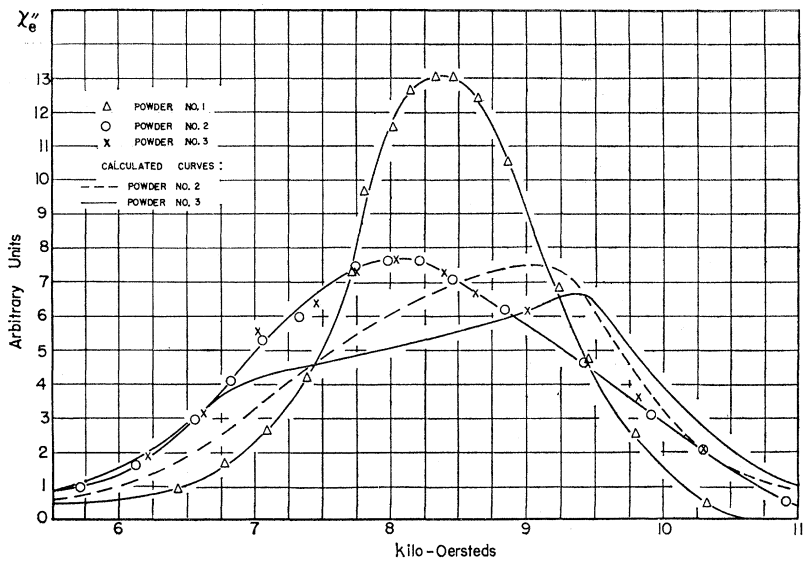

FIG. 12. Theoretical and experimental results for 24 116 Mc/sec.

line width.[33] In order to determine H_r as accurately as possible, spherical samples of different diameters were used and the measured resonance fields extrapolated to zero diameter.[34]

The experimental data are shown in Table I. Using $M_s=370$ emu/cm^3, one finds: $g=1.97\pm0.02$, $K_1=-2.9\times10^5$ ergs/cm^3, $\tau=1.2\times10^{-10}$ sec.

TABLE I. Experimental data for powder I.

f (Mc/sec)	H_r (Oe)	ΔH (Oe)
9480	3050	1750
24 116	8360	1725

CONCLUSIONS

In order to obtain agreement between theory and experiment, a value for the crystalline anisotropy constant $|K_1|$ of approximately 2.5×10^5 ergs/cm^3 has to be assumed for γ-Fe_2O_3. This estimate was arrived at in two independent ways: (a) by fitting the theoretical curves to the experimental data for $H_e=0$, and (b) by using Eq. (23) and the experimental results at 9840 and 24 116 Mc/sec. According to microscopic theories of the crystalline anisotropy, the directional effects arise because of the spin-orbit coupling. Now γ-Fe_2O_3 contains only ferric ions, which have a ground state with $L=0$. Hence, our value of $|K_1|$ appears to be rather large. It would be pertinent to conduct ferromagnetic resonance experiments on single crystals of γ-Fe_2O_3. However no one has yet succeeded in growing such crystals. Resonance experiments on the powders with $H_e=0$ at other temperatures would also be informative. Since both the shape anisotropy and interaction energy terms are proportional to the square of the magnetization while the crystalline anisotropy energy is proportional to a high (perhaps the tenth) power of the magnetization, a better separation of these terms might then be possible. For the present, the value of 2.5×10^5 erg/cm^3 for γ-Fe_2O_3 should be considered as representing a phenomenological anisotropy constant.

With great certainty, 1.2×10^{-10} sec can be assumed to be a lower limit of τ for γ-Fe_2O_3, the true value presumably being around 2.0×10^{-10} sec.

For zero applied steady field, there is reasonable agreement between experiment and a theory which is based on the Stoner-Wohlfarth[1] model, even when crystalline anisotropy and particle interactions are neglected. This is in sharp contrast to some other experiments that involve magnetization reversals in the single-domain particles, such as measurements of the coercive force and remanence.[3-7] Thus our results provide indirect support for the existence of these reversal modes.

In the absence of an applied steady field, good agreement between theory and experiment can only be achieved when particle interaction is taken into account. This can be done in a rough fashion by assuming an effective shape distribution, and qualitative arguments have been given to justify this approach. It has not been attempted to find a way of deriving the effective shape distribution from the actual one; but it has been shown that, for acicular powders, the average effective shape factor is smaller than the average shape factor of the isolated particles, and that this effective reduction of the shape factor is the greater, the greater the acicularity of the powder. For powders with close to spherical particle shape, good results were obtained assuming an effective shape distribution with an average axial ratio of 1.8:1, the effective particle shape being considered as spheroidal.

[33] A. H. Morrish and E. P. Valstyn, J. Phys. Soc. Japan **17** Suppl. BI, 392 (1962).
[34] W. A. Yager, F. R. Merritt, and C. Guillaud, Phys. Rev. **81**, 477 (1951).

ACKNOWLEDGMENTS

We wish to thank W. F. Brown, Jr., for important contributions in the early part of the theoretical work and for helpful discussions. We are also indebted to W. E. Swanson for considerable assistance with the experimental measurements.

APPENDIX

Typical Minima of $F=F_N+F_K$ and Values of f_0

Some typical equilibrium orientations of **M** and the corresponding resonance frequencies, f_0, are tabulated for two particle orientations: Table II, $\alpha=0°$, $\beta=30°$ and Table III, $\alpha=20°$, $\beta=30°$. The axial ratios are those of prolate spheroids. $M_s=390$ emu/cm^3, $K_1=-3.0\times10^5$ ergs/cm^3, and $g=2$. Only four octants are listed, since, on account of the symmetry, octants 1 and 7 are equivalent, and so are octants 2 and 8, 3 and 5, and 4 and 6. (The octants are numbered from 1 to 4 with increasing azimuth in the upper hemisphere and in the lower hemisphere from 5 to 8 such that 5 borders with 1, 6 with 2, etc.) Whenever one of octants 1 through 4 is not listed for a certain axial ratio, it does not contain an energy minimum.

TABLE II. Typical equilibrium orientations of **M** and resonance frequencies, f_0, for $\alpha=0°$, $\beta=30°$.

Axial ratio	Octant	ϕ_0 (degrees)	θ_0 (degrees)	f_0 (kMc/sec)	Labeling in Fig. 6
1.00	1	45.00	54.74	2.87	A
1.00	2	135.00	54.74	2.87	A
1.00	3	225.00	54.74	2.87	A
1.00	4	315.00	54.74	2.87	A
1.10	1	40.92	50.95	3.00	B
1.10	2	133.74	52.46	2.62	B
1.10	3	226.26	52.46	2.62	B
1.10	4	319.08	50.95	3.00	B
1.20	1	36.25	47.93	2.93	C
1.20	2	131.64	49.74	2.30	C
1.20	3	228.36	49.74	2.30	C
1.20	4	323.75	47.93	2.93	C
1.30	1	30.90	45.36	2.70	D
1.30	2	126.99	45.96	1.61	D
1.30	3	233.01	45.96	1.61	D
1.30	4	329.10	45.36	2.70	D
1.35	1	27.89	44.21	2.51	E
1.35	4	332.11	44.21	2.51	E
1.40	1	24.54	43.13	2.27	F
1.40	4	335.46	43.13	2.27	F
1.50	1	16.02	41.15	1.56	G
1.50	4	343.98	41.15	1.56	G
1.54	1	10.97	40.42	1.08	H
1.54	4	349.03	40.42	1.08	H
1.58	1, 4	0.00	39.76	0.27	I
1.60	1, 4	0.00	39.68	0.64	I
1.64	1, 4	0.00	39.51	1.04	I
1.70	1, 4	0.00	39.29	1.43	I

TABLE III. Typical equilibrium orientations of **M** and resonance frequencies, f_0, for $\alpha=20°$, $\beta=30°$.

Axial ratio	Octant	ϕ_0 (degrees)	θ_0 (degrees)	f_0 (kMc/sec)
1.00	1	45.00	54.74	2.87
1.00	2	135.00	54.74	2.87
1.00	3	225.00	54.74	2.87
1.00	4	315.00	54.74	2.87
1.10	1	42.49	51.25	3.15
1.10	2	132.43	51.61	2.63
1.10	3	225.45	53.22	2.62
1.10	4	319.84	50.72	2.83
1.20	1	40.08	48.76	3.33
1.20	2	127.56	47.82	2.09
1.20	3	226.14	51.37	2.36
1.20	4	327.19	46.85	2.34
1.30	1	37.91	46.88	3.48
1.30	3	227.25	49.11	2.08
1.40	1	36.03	45.43	3.62
1.40	3	229.41	46.13	1.67
1.46	1	35.04	44.71	3.70
1.46	3	232.78	43.30	1.07
1.48	1	34.73	44.49	3.73
1.50	1	34.43	44.28	3.75
1.60	1	33.09	43.36	3.89
1.70	1	31.97	42.61	4.03

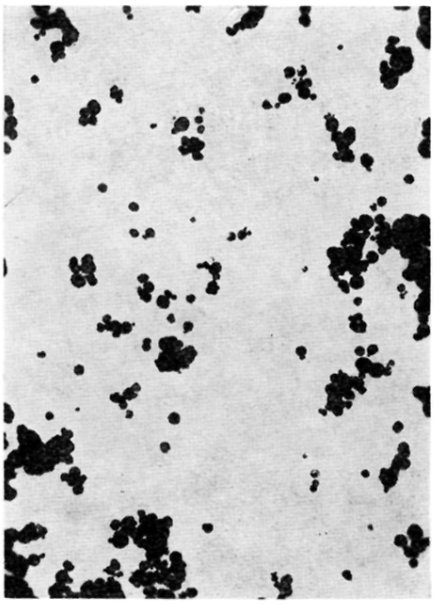

FIG. 1. Electron photomicrograph of powder 1.
Magnification 16 150×.